Steady Detonation in Gaseous Pyrolysis Products of Ammonium Dinitramide and its related Ionic Liquids

Noboru Itouyama and Jiro Kasahara
Nagoya University, Nagoya, Aichi, Japan

Xiangrong Huang and Rémy Mevel
Center for Combustion Energy, Tsinghua University, Beijing, China

1 Introduction

Ammonium dinitramide (ADN) is one high-energy density material (HEDMs), which was widely investigated as a monopropellant for propulsion systems [1]. Recently, newer ADN-based monopropellant called "Energetic Ionic Liquid Propellant (EILPs)" were developed [2], with the benefits that no solvent is included in such compounds, and that the propulsion potential is about 1.5 times higher. Since HEDMs and EILPs contains very large amount of energy, they presents a significant risk and accidental combustion events involving such compounds might have dramatic consequences. The most hazardous combustion event that could take place in HEDMs corresponds to a detonation. Since HEDMs include both fuel and oxidizer components in their chemical skeletons, they have the potential to burn or detonate alone (without any oxidizer). Typically, HEDMs can sustain detonation in their solid or condensed-phase and such detonation phenomena are well-investigated [3]. On the contrary, the investigations of gaseous detonation related to HEDMs are quite scarce. The gaseous species originating from HEDMs and their derivatives correspond to their decomposition or evaporation products. The resulting gas mixture is combustible and might have an important explosive potential. Therefore, it is of the primary importance to study the properties of a gas-phase detonation propagating in the decomposition products of ADN and ADN-based propellant.
The goal of the present study is to estimate the detonation sensitivity of the gaseous decomposition products formed during the pyrolysis of ADN and some ADN-based propellants through steady detonation simulation performed with a detailed reaction model. Especially, the study focuses on the scenario that the combustion of AMU442 along with thermal decomposition goes on its runaway (transition to detonation).

2 Modeling approach and calculated targets

2.1 Reaction and detonation models

The detailed reaction model of ADN-EILPs is composed of 894 reactions and 113 species [5]. Reaction rate constants were checked for collision limit violation in the range 1500-3200 K using [6]. Few reaction rate constants found slightly above the limit were either replaced by other constants from the literature, or reduced to respect this limit, without inducing significant modifications of the predictions.

Correspondence to: itouyama@imass.nagoya-u.ac.jp

We have employed a Chemkin II implementation of the ZND theory of steady detonation, similar to [7]. Along with the perfect gas equation of state, the system of equations is

$$\frac{dY_i}{dx} = \frac{\omega_i}{\rho u} \quad ; \quad \frac{du}{dx} = \frac{\sigma}{1-M^2} \quad ; \quad \frac{dP}{dx} = -\rho u \frac{\sigma}{1-M^2} \quad ; \quad \frac{d\rho}{dx} = -\frac{\rho}{u}\frac{\sigma}{1-M^2}, \tag{1}$$

where Y is the mass fraction; x is the spatial coordinate; ω_i is the chemical source term; ρ is the density; u is the velocity; σ is the thermicity; M is the Mach number; and P is the pressure.

2.2 Selection of initial conditions

We focus on ADN and ADN-based EILPs. EILPs are composed by three solid materials, ADN, monomethylamine nitrate (MMAN) and urea. Especially, the EILPs with the weight ratio of ADN:MMAN:urea = 40:40:20 (named AMU442) has been investigated extensively and was selected as an ADN-based monopropellant. ADN and EILPs are generally consumed through their thermal decomposition or combustion. These processes are characterized by a change from condensed to gas-phase. We assumed a detonation has been initiated in the gaseous decomposition products of ADN and ADN-based EILPs.

For both ADN and AMU442, a correlation exists between the pressure and temperature at which their decomposition is taking place [8, 9] and can be expressed as an Antoine formula-like relation given as

$$\log P = 1.2449 \times 10 - \frac{4.5474 \times 10^3}{T} \tag{2}$$

To apply Equation 2 and obtain the corresponding temperature at which ADN and AMU442 would vaporize, two pressures were selected and correspond to general operation pressures for HEDMs' consumptions (e.g. gas generators or chemical propulsion) or handling in laboratories. The two set of initial conditions obtained were: 1) T_1=705 K and P_1=1.0 MPa and 2) T_1=610 K and P_1=0.1 MPa.

Table 1: Compositions, in mole fraction, employed in the present study.

mixture	HDN	HNO_3	NH_3	N_2O	NO
1	0.031	0.082	0.112	0.224	0.163
2	0.016	0.219	0.057	0.114	0.083
	N_2	H_2O	CH_3NH_2	CH_4N_2O	Elem comp (H:O:N:C)
1	0.082	0.306	0	0	1:1:1
2	0.041	0.155	0.177	0.139	1:0.56:0.54:0.15

Following the selection of the initial state, it is needed to determine the corresponding mixture compositions. Assumed that the scenario the steady combustion of AMU442, two mixture compositions, given in Table 1, were obtained indirectly by comparing experimental combustion data such as the flame structure and the surface regression rate with calculated results. The compositions that enables to match at best the experimental data were selected from further investigation using the ZND simulations. It is noted that not all the decomposition products can be identified experimentally or included in the simulation, which results in a possible miss-match between the elemental composition of the condensed-phase and of the gas-phase phase.

Considering two target compositions, a total of four cases of steady detonation calculations for ADN and AMU442 were studied: (1) Case 1 is with mixture 1 of gas composition, 705 K of initial gas temperature, and 1.0 MPa of initial gas pressure; (2) Case 2 is with mixture 1 of gas composition, 610 K of initial gas temperature, and 0.1 MPa of initial gas pressure, (3) Case 3 is with mixture 2 of gas composition, 705 K of initial gas temperature, and 1.0 MPa of initial gas pressure, and (4) Case 4 is with mixture 2 of gas composition610 K of initial gas temperature, and 0.1 MPa of initial gas pressure.

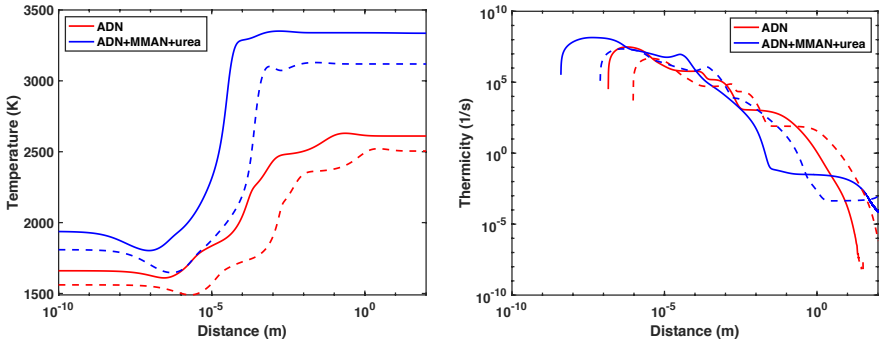

a) Temperature b) Thermicity

Figure 1: Temperature and Thermicity ZND profiles obtained for mixtures 1 and 2. Solid lines: high-pressure cases. Dashed lines: low-pressure cases.

3 ZND structure

Figure 1 shows the temperature, and thermicity ZND profiles for the two mixtures and two sets of initial conditions. For both mixtures, the shape of the temperature and thermicity profiles are similar at low and high pressure while higher reactivity is observed at high pressure. In all cases, the reaction is initiated by an important and rapid endothermic step which results in the drop of temperature in the induction zone. Such a feature is usually observed for mixtures with a low level of dilution and is a result of the reactant thermal decomposition [10]. The temperature profiles demonstrate peaks of temperature slightly higher than the Chapman-Jouguet temperatures. This feature seems related to a super-equilibrium with a production of water at a concentration above the equilibrium one. Under such conditions, water decomposes which induces a drop of temperature. Nitrogen does not demonstrate such a super-equilibrium behavior but two main steps of productions are observed for mixture 1. For mixture 1, up to four steps of temperature increase are observed but are not necessarily associated with peaks of thermicity since only one peak exists at high pressure and only two peaks exist at low pressure. For mixture 2, two peaks of thermicity can be clearly identified, both at high and low pressure. Two-step heat release has been reported in a variety of mixtures including nitromethane and nitromethane-oxygen [10]; H_2-NO_2/N_2O_4 [11], CH_4 or C_2H_6-N_2O/N_2O_4 [11], H_2-N_2O [12], dimethyl ether-oxygen [13]. For low-temperature affected detonation [14], up to three steps of energy release were observed. Detonations in type Ia supernovae are believed to demonstrate multi-level structure [15]. Under specific conditions, mixtures with two steps of heat release may exhibit complex cellular structure referred to as double cellular structure [10].

The induction length in the ZND solution is well-known to correlate with the size of detonation cell, see for example the proportional relation found by Ng *et al.* [16]. Generally, induction length is defined using thermicity peaks. In this study, it is difficult to reveal which induction length contributes most to the formation of the cell structure. Nevertheless, we have measured the different induction lengths visible in Figure 1. The results are tabulated in Table 2 with the predicted activation energy. For both mixtures, all induction lengths become shorter as pressure increases. At high-pressure conditions and considering the distance to the absolute peak thermicity, the induction zone length was found to be below 0.65 μm for the ADN-based mixture, and below 0.05 μm for the AMU442-based mixture. In addition, the chemical reaction length, defined as the distance needed for the thermicity profile to drop below 1 s^{-1}, was also shorter for mixture 2 than for mixture 1. Still at high pressure, for the ADN mixture, the overall length of reaction is on the order of 1 m, whereas for the AMU442-based mixture, the overall length of reaction is on the order of 10 cm. It is not clear if the two mixtures we presently

Table 2: Characteristics length-scale and detonation parameters for cases 1 to 4. Δ_i: induction length; θ: reduced activation energy at vN state.

Case No.	peak No.	Δ_i (μm)	θ	Case No.	peak No.	Δ_i (μm)	θ
1	1^{st}	0.631	6.64	3	1^{st}	0.047	9.02
	2^{nd}	-			2^{nd}	35	
2	1^{st}	3.614	4.81	4	1^{st}	0.428	8.17
	2^{nd}	1517			2^{nd}	240	

studied would demonstrate multi-level detonation structure and two-dimensional numerical simulation and experimental soot foil would be required to study this aspect.

4 Thermo-chemical analyses

To better understand the difference of detonation length-scale between the ADN- and AMU442-based mixtures, the chemical dynamics were investigated through energy release rate and sensitivity analyses.

The energy release rate profiles are shown in Figure 2 a) for mixture 1. For both mixtures, the thermal decomposition of HNO_3 corresponds to the dominant process within the induction zone, consistent with [5], and is responsible for the drop of temperature observed during the initial stage of the reaction. For mixture 1, the ERR profile of HNO_3 decomposition demonstrates two changes of slope which participate to the non-monotonous temperature profile. The energy release is dominated by three reactions: $HNNO_2$+NO=N_2O+HNO_2; NH_2+NO=N_2+H_2O; OH+HO_2=H_2O+O_2. In addition, the reaction NH_3+OH=NH_2+H_2O also plays a significant role. For mixture 2 (not shown), the ERR profile of nitric acid does not demonstrate a complex shape and the energy release is dominated by CH_3NH_2+OH=CH_2NH_2+H_2O, and CH_3NH_2+OH= CH_3NH+H_2O.

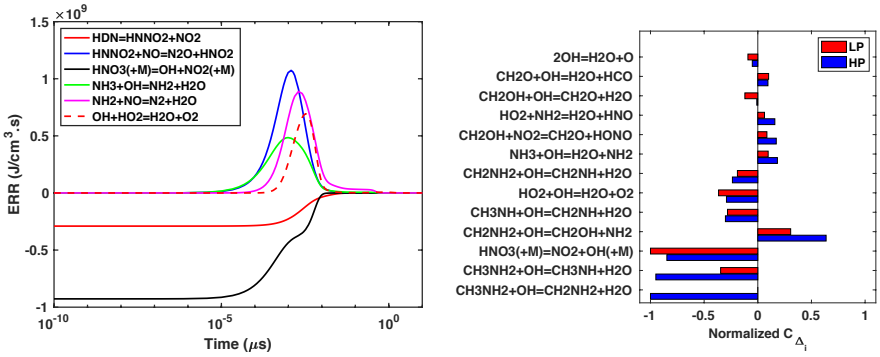

a) ERR for mixture 1 b) Sensitivity for mixture 2

Figure 2: a) Energy release rate profiles and b) Sensitivity coefficient on the induction length obtained under ZND conditions for mixtures 1 and 2 initially at 705 K and 1 MPa. The ERR for the reaction HNO_3(+M)=OH+NO_2(+M) have been divided by 10.

The sensitivity coefficients on Δ_i are shown in Figure 2 b) for mixture 2. The results obtained for the low- and high-pressure cases are relatively similar but some differences exist: (i) for mixture 1 (not shown), the sensitivity coefficient for the reaction HDN=$HNNO_2$+NO_2 is much larger at low pressure; (ii) for mixture 2, the induction length is more sensitive at high pressure to the reactions between CH_3NH_2 or CH_2NH_2 and OH. For mixture 1, the most sensitive reactions all demonstrate a negative

sensitivity coefficient, indicating that increasing their rate constant promotes reactivity and lead to a reduction of Δ_i. At high pressure, case 1, the most sensitive reactions are HNO_3(+M)=NO_2+OH(+M), HDN+OH=$HNNO_2$+HNO_3, HDN+NH_2=$HNNO_2$+NH_2NO_2, and HO_2+NO=NO2+OH. At low pressure, case 2, the most sensitive reaction is HDN=$HNNO_2$+NO_2, whereas the reaction HNO_3(+M)=NO_2+OH(+M) becomes the second most sensitive reaction. For mixture 2, several reactions demonstrate noticeable positive sensitivity coefficients, which indicates that increasing their rate constant lead to a lower reactivity and an increase of the induction zone length. The most sensitive reactions are those between CH_3NH_2 or CH_2NH_2 and OH whereas HNO_3(+M)=NO_2+OH(+M) also demonstrates a very high negative coefficient. This sensitivity analysis demonstrate the predominant role of the decomposition of HNO_3, which rapidly releases very reactive hydroxyl radicals.

5 Uncertainty quantification

To evaluate the reliability of the ZND simulations, in particular for the induction length calculations, we have performed an uncertainty quantification (UQ) study for cases 1 and 3. Two of the most sensitive reactions in each case were selected to apply the UQ approach as described in [17], which consists in the following four steps: (i) determine the level of uncertainty for the pre-exponential factor (A) of the reaction rate (model input); (ii) perturb randomly the model input by applying a Monte Carlo sampling approach; (iii) calculate the induction length (model output) with the perturbed model input; and (iv) statistically interpret the distribution of the model output. The uncertainty on the rate constant is commonly characterized by the uncertainty factor (u) or the uncertainty parameter (f). The definition of u is $u = k_0/k_{min} = k_{max}/k_0$, where k_0 is the nominal rate constant; k_{min} and k_{max} are the minimal and maximal values of k_0. f is defined as the base-10 logarithm of u, $f = \log_{10} u = 3\sigma/\ln 10$, where σ is the variance of the normal distribution that $\ln A$ was assumed to follow. For each reaction, the rate constant was sampled 10,000 times and the uncertainty on Δ_i was characterized by the standard deviation (σ_Δ).

Figure 3 shows the distributions of induction length calculated as model output. For case 1, the largest uncertainty is induced by the uncertainty on the rate constant of the decomposition reaction of HNO_3. For this reaction, the standard deviation represents approximately 13% of the mean value. The distributions obtained when perturbing the rate of R5 has a standard deviation around 5.4%. For case 3, the uncertainties on R885, and R886, lead to similar standard deviation around 18% of the mean value. Considering the spreading of the results calculated with perturbed model input, it could be concluded that the uncertainty on the induction zone length is of approximately 50%.

Table 3: Uncertainties propagating from the uncertainties of the rate constant of top sensitive reactions in prediction induction length. a: Uncertainty factor. b: Uncertainty parameter. c: f was assumed based on [17]. d: Average value of induction length for all samples. e: Uncertainty of induction length.

N°	Reaction	Case	u^a	f^b	Source	μ^d (mm)	σ^e_Δ (mm)
28	HNO_3 (+M) <=> NO_2 + OH (+M)	1	3.16	0.5	Assumed^c	6.4E-07	8.21E-08
5	HDN + OH <=> $HNNO_2$ + HNO_3	1	3.16	0.5	Assumed^c	6.3E-07	3.40E-08
885	CH_3NH_2 + OH <=> CH_2NH_2 + H_2O	3	3.16	0.5	Assumed^c	4.4E-08	7.66E-09
886	CH_3NH_2 + OH <=> CH_3NH + H_2O	3	3.16	0.5	Assumed^c	4.6E-08	8.24E-09

References

[1] Matsunaga H, Habu H, Miyake A. (2013). J. Therm. Anal. Cal. 111: 1183.

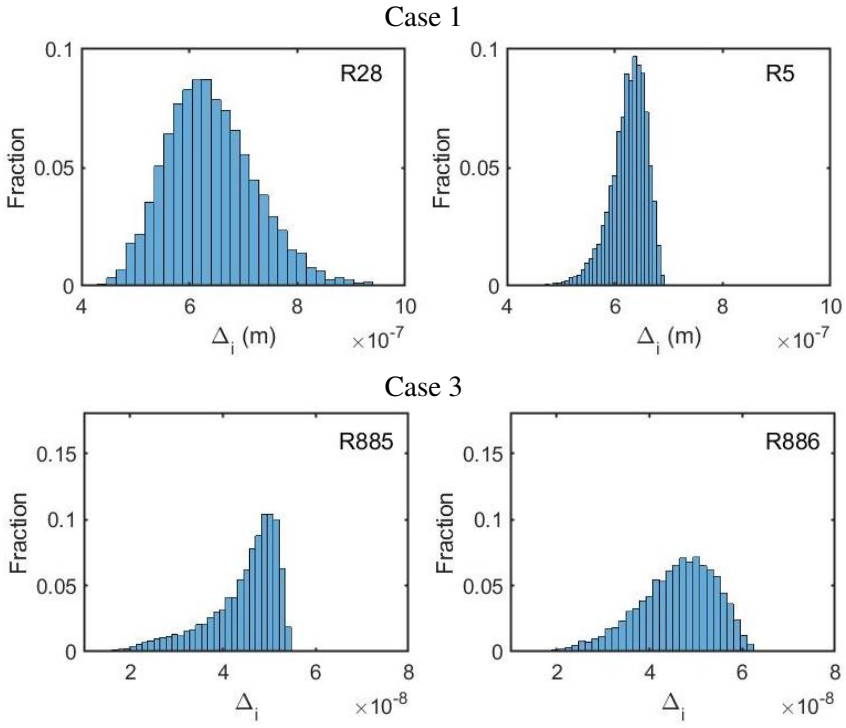

Figure 3: Distribution of ZND Δ_i obtained by perturbing 10,000 times each rate constant for two of the most sensitive reactions. Results were obtained for mixtures 1 and 2 initially at 705 K and 1 MPa.

[2] Matsunaga H, Habu H, Miyake A. (2017). Sci. Technol. Energ. Mat. 78: 65.

[3] Mathieu D. (2017). Indust. Eng. Chem. Res. 56: 8191.

[4] Li C, Li H, Zong H, Huang Y, Gozin M, Sun C, Zhang L. (2020). iScience. 23: 100944.

[5] Itouyama N, Izato Y, Miyake A, Habu H. (2020). Sci. Technol. Energ. Mat. 81: 53.

[6] Yalamanchi K, Tingas EA, Im H, Sarathy S. (2020). Int. J. Chem. Kinet. 52: 599.

[7] Shepherd JE. (1986). Progr. Astronaut. Aero. 106: 263.

[8] Ide Y. (2017). Experimental Study on Combustion of ADN-based Ionic Liquid. Ph.D thesis: the Graduate University for Advanced Studies.

[9] Sinditskii VP, Egorshev VY, Serushkin VV, Filatov SA. (2012). Combust. Explos. Shock+. 48: 81.

[10] Sturtzer MO, Lamoureux N, Matignon C, Desbordes D, Presles H. (2005). Shock Waves. 14: 45.

[11] Joubert F, Desbordes D, Presles H. (2008). Combust. Flame. 152: 482.

[12] Davidenko D, Mével R, Dupré G. (2011). Shock Waves. 21: 85.

[13] Ng H, Chao J, Yatsufusa T, Lee J. (2009). Fuel. 88: 124.

[14] Liang W, Mével R, Law C. (2018). Combust. Flame. 193: 463.

[15] Gamezo V, Wheeler J, Khoklov A, Oran E. (1999). Astrophys. J. 512: 827.

[16] Ng HD, Ju Y, Lee JHS. (2007). Int. J. Hydro. Ener. 32: 93.

[17] Nagy T., Valko E., Sedyo I., Zsely I.G., Pilling M.J., and Turanyi T. (2015). Combust. Flame **162**: 2059.

[18] Baulch D.L. et al. (2005). J. Phys. Chem. Ref. Data **34**: 757.